



## EFFECTS OF SPRAY CONE ANGLE ON COMBUSTION AND PERFORMANCE CHARACTERISTICS OF DIRECT INJECTION ENGINE FOR KEROSENE

Ahmet Alper YONTAR

Princeton University, School of Engineering and Applied Science, Department of Mechanical and Aerospace Engineering, Princeton, New Jersey 08544, U.S.A., ayontar@princeton.edu

(Geliş Tarihi: 22.03.2019, Kabul Tarihi: 28.09.2019)

**Abstract:** This study focuses on the determination of the effects of spray cone angles on in-cylinder combustion characteristics for kerosene via numerical and experimental methods. For this aim, the 3-D in-cylinder combustion CFD (Computational Fluid Dynamics) analyses were employed in the determination of engine characteristics at full load position. Also, the engine tests were performed using injectors with different spray cone angles. Measured performance parameters and numerical results were compared. The closed cycle CFD analyses; the engine speed, excess air coefficient and compression ratio were kept constant at 1300 rpm, 1.7 and 17:1, respectively. The 3-D in-cylinder CFD analyses were performed in Star-CD/es-ice software for kerosene. The CFD model was built by using RNG equations, k-ε turbulence model, and ECFM-3Z/Compression combustion model. The closed cycle was defined in the range of 40 CAD before top dead center to 80 CAD after top dead center. Spray cone angle (SCA) was changed in the range of 5°-25° and analyzed in 5° steps at the intervals. The results show that the in-cylinder pressure at 20° SCA is 15.8% higher than 5° SCA. The indicated mean effective pressure at 20° SCA was observed as 4.06% and 3.41% higher than 5° SCA and 25° SCA, respectively. The temperature in-cylinder increased to 5°-20° SCA while the highest temperature rises from 1620 to 1720 K in-cylinder. The indicated power at 20° SCA was detected as 7.98% and 6.72% higher than 5° SCA and 25° SCA, respectively. The brake specific fuel consumption at tests for 20° SCA is 8.51% and 7.23% lower than 5° SCA and 25° SCA. The CO<sub>2</sub> formation at 20° SCA is overall 24.3% higher than 5° SCA. The NO<sub>x</sub> formation for 25° SCA is higher 51.2% than 5° SCA and 19.2% lower than 25° SCA. The soot formation at 20° SCA is overall 24.8% lower than 5° SCA. As a result of the study, the optimum spray cone angle for the operating conditions specified in the kerosene usage was determined to be 20° SCA.

**Keywords:** Spray cone angle, kerosene, droplet velocity, direct injection engine, soot.

## SPREY KONİ AÇISININ DİREKT ENJEKSİYONLU MOTORDA KEROSEN İÇİN YANMA VE PERFORMANS KARAKTERİSTİKLERİNE ETKİLERİ

**Özet:** Bu çalışma, sprey koni açılarının silindir içi yanma özellikleri üzerindeki etkilerinin kerosen kullanımı için sayısal ve deneysel yöntemlerle belirlenmesi üzerine odaklanmıştır. Bu amaçla, 3-B silindir içi yanma HAD (Hesaplamalı Akışkanlar Dinamiđi) analizleri, tam yük konumunda motor karakteristiklerinin belirlenmesinde kullanılmıştır. Ayrıca motor testleri, farklı püskürtme konisi açılara sahip enjektörler kullanılarak yapıldı. Ölçülen performans parametreleri ve sayısal sonuçlar karşılaştırıldı. Kapalı çevrim HAD analizlerinde sırasıyla; motor hızı 1300 d/dak, hava fazlalık katsayısı 1,7 ve sıkıştırma oranı 17:1 olarak sabit tutuldu. 3-B silindir içi HAD analizleri Star-CD/es-ice yazılımında kerosen kullanımı için gerçekleştirildi. HAD modeli; RNG denklemleri, k-ε türbülans modeli ve ECFM-3Z/Compression yanma modeli kullanılarak oluşturulmuştur. Kapalı çevrim çözüm aralığı; üst ölü nokta sıfır kabul edilecek şekilde, üst ölü noktadan 40 KMA önce ile üst ölü noktadan 80 KMA sonra aralığında tanımlandı. Sprey koni açıları (SKA) 5°-25° aralığında değiştirildi ve 5°'lik adımlarla bu aralıkta analizler gerçekleştirildi. Sonuçlar 20° SKA'da 5° SKA'ya göre silindir içi basıncın %15,8 yüksek olduğunu göstermektedir. İndike ortalama efektif basıncın 20° SKA'da; sırasıyla 5° SKA'ya ve 25° SKA'ya göre %4,06 ve %3,41 yüksek olduğu gözlemlendi. Sprey koni açısı 5°'den 20°'ya artarken silindir içi sıcaklık 1620 K'den 1720 K'e yükseldi. İndike güç 20° SKA'da; 5° SKA'ya ve 25° SKA'ya göre sırasıyla, %7,98 ve %6,72 yüksek olduğu tespit edildi. Testlerde özgül yakıt sarfiyatı 20° SKA'da 5° SKA'ya ve 25° SKA'ya göre %8,51 ve %7,33 daha düşüktür. Genel olarak 20° SKA'daki CO<sub>2</sub> oluşumu, 5° SKA'dan %24,3 daha yüksektir. 25° SKA için NO<sub>x</sub> oluşumu 5° SKA'dan %51,2 ve 25° SKA'dan %19,2 daha düşüktür. 20° SKA'da kurum oluşumu genel olarak 5° SKA'dan %24,8 daha düşüktür. Çalışmanın sonucunda kerosen kullanımında belirtilen çalışma koşulları için optimum püskürtme konisi açısı 20° SKA olarak belirlenmiştir.

**Anahtar Kelimeler:** Sprey koni açısı, kerosen, damlacık hızı, direkt enjeksiyonlu motor, is.

## INTRODUCTION

Energy efficiency and environmental impacts influence the development of engine technology as much as competition for automotive companies. Today's level of technology makes it possible for theoretical ideas to quickly take place in commercial engines after laboratory testing. In addition to the rapidly developing engine technology, the engines are designed to be optimized for specific fuel and are being used with different fuels to reduce fuel consumption costs and reduce environmental impacts. In those cases where alternative fuels are employed instead of the original design fuel of the engine, the engine behavior is known as well as the optimum setting of the engine settings for the alternative fuel remains on the agenda.

The most important parameters for compression-ignition engines are the injection timing and the characteristics of the spray injected from the injector. The fuel injection into the cylinder with optimum spray properties has a significant impact on engine performance and emissions. The determination of the optimum spray properties for the engine and fuel requires inspection of the in-cylinder combustion.

The spray properties determination for alternative fuel usage in the engine designed is also important for engine characteristics and environmental pollution. In the literature, the studies on the effects of spray properties by experimental and numerical methods are quite limited for alternative fuels used in commercial engines (Sovani et al., 2001; Langrish and Zbicinski, 1994; Ohn et al., 1991; Chen and Lefebvre, 1994; Varde et al., 1984; Kim and Lee, 2007; Juslin et al., 1995; Patterson and Reitz, 1998). The selection of optimum spray properties as a precursor by numerical methods is important in terms of cost, time and efficiency.

Spray characteristics are experimentally measured and determined by macroscopic and microscopic methodologies such as spray penetration length, spray cone angle, droplet distribution, droplet velocity etc. (Delacourt et al., 2005; Verhoeven et al., 1998, Suh et al., 2007; Doudou, 2005; Hwang et al., 2003; Desantes et al., 2007; Payri et al., 2005). To make these measurements requires a strong laboratory infrastructure. The many researchers proposed and enhanced the equations about spray cone angle, spray penetration length and break-up length (Wakuri et al., 1960; Dent, 1971; Hiroyasu and Arai, 1990; Kostas et al., 2009; Naber and Siebers, 1996; Roisman et al., 2007; Dec, 1997). High injection pressure is used today's internal combustion engines injection systems and too high-pressure values cause cavitation problem. Therefore, it is important to determine the spray geometric properties for direct injection combustion engines. The injector nozzle geometry widely effects on spray development and ignition delay time. The ignition delay time is another important parameter for

compression-ignition engine. In this context, some studies on the subject and in the literature are given below.

Watanabe et al. (2007), investigated simulation analysis for spray combustion. They employed  $k-\epsilon$  turbulence in turbulence spray combustion model and detailed to examine soot and  $\text{NO}_x$ . Their calculated results are compared with experimental data to demonstrate the validity of the numerical model. They observed that the temperature without soot radiation was higher than the experimental data. They detected that the soot formation greatly affects heat transfer on the jet burner.

Nakamura et al. (2011), experimentally studied coaxial jet spray flames for kerosene. They detailed investigate flame structure, droplet behavior and soot formation region which varies with changes in pressure. Their results showed that high-temperature regions appear near the burner. They demonstrated when pressure increases, the peak of soot volume fraction appears at the central axis and moves upstream.

Von Berg et al. (2005) investigated two approaches nozzle flow for coupled simulations. They used AVL FIRE computational fluid dynamics code to obtain the results. They have been developed a new simulation methodology for the spray formation and primary breakup model. Their spray formation analyzes results show similar trends with experimental data in the literature.

Hossainpour and Binesh (2009), modeled IC-engine fuel spray formation and propagation processes. They employed Chu model, Reitz and Diwakar model, Wave model, Kelvin-Helmholtz and Rayleigh-Taylor model in their study and compared break-up models with experimental data in the literature. They observed that Chu model predicts the spray tip penetration comparing with predictions obtained from other models. The ignition delay and ignition timing accurately were captured by all the spray breakup models.

Aleiferis et al. (2010), investigated using a multi-hole injector for the spray formation and combustion characteristics of gasoline and E85 (85% ethanol, 15% gasoline) via experimental methodology. They studied the effect of fuel properties on vaporization and mixture preparation. They detected that spray formation was more insensitive to changes in temperature and pressure for E85 compared to gasoline and the droplet sizes of E85 were larger than gasoline.

Mitroglou et al. (2006), numerically studied spray characteristics effect for direct-injection gasoline engines. They detected spray angle be almost independent of injection and chamber pressure for multi-hole Injector. Their results showed that droplet velocities increase sharply at the start of injection and then to remain unchanged during the main part of

injection. They measured the effect of injection pressure on the droplet size range. The droplet size decreased while the increase in chamber pressure.

Skogsberg et al. (2005), investigated injector parameters effects on mixture formation for gasoline direct injection engine. Their study had been done numerically using AVL Fire and experimentally using laser diagnostic. The experimentally and numerically results showed that the spray's high axial velocity caused the umbrella angle to be reduced for the injection period. They reported about the umbrella angle may be an important parameter to decrease hydrocarbon emission formation. Their experimentally measurements showed that the spray angle formation is not affected by variations in either density or temperature of the surrounding gas.

Patterson and Reitz (1998), modeled fuel spray for a diesel engine using with KIVA-II CFD code. They investigated to spray characteristics effects on combustion and emission. They validated their results with experimental data. Their spray model for heavy-duty diesel engine improved combustion predictions and early injection cases. The spray model compared to experimental data that it showed a more accurate calculation for droplet size and heat release.

Wang et al. (2010), carried out an experimental and analytical study for diesel spray characteristics. They investigated ultra-high injection pressure for biodiesel usage. Their study demonstrated that biodiesels give longer injection delay, spray tip penetration and smaller spray angle than diesel fuel. In addition, they detected spray droplet size for biodiesels generate larger Sauter mean diameter due to higher viscosity and surface tension.

Arrègle et al. (1999), investigated injection parameters effects on diesel spray characteristics. They carried out a detailed study of microscopic and macroscopic behaviors. They detected that the spray cone angle is independent of the injection pressure on the other hand it changes significantly with the gas density.

Agarwal and Chaudhury (2012), investigated spray characteristics at high-pressure constant volume chamber for biodiesel and blends. Their experimental investigation results showed that spray tip penetration decreases and spray cone angle increases as the chamber pressure rises up.

Park et al. (2011), conducted an experimental study and examined the effects of multiple injections. Their single cylinder diesel engine test study included the free spray characteristics and in-cylinder spray behaviors of the multiple-injection modes. The results demonstrated that multiple-injection modes have a higher IMEP than the single-injection mode. In addition, a short injection interval induced a decrease in soot, HC, and CO emissions, while NO<sub>x</sub> emission increased. They showed

the multiple-injection modes were used in a diesel engine and the number of large particles significantly decreased compared to single-injection combustion.

Battistoni and Grimaldi (2012), investigated injector flow and spray characteristics via numerical methodology. They compared the injection process of diesel fuel and biodiesel fuel. In this study, fuel property effects were investigated for density, viscosity and vapor pressure. They observed that biodiesel produces larger droplet diameters and slower breakup process. They demonstrated spray cone-angle are significantly affected by hole shape for diesel than biodiesel.

Park et al. (2009), carried out atomization and spray characteristics study for bioethanol and bioethanol blended gasoline fuel. They used experimental and numerical methods for direct injection gasoline injector investigation. They detected an increase of the injection pressure caused a circular shape of the downstream spray. In addition, it caused a uniform mixture between the injected spray droplets and ambient air. Their results showed that the spray width and the cone angle of ethanol were slightly larger than gasoline and E85 fuels.

Liu et al. (2013), carried out a numerical study for pressure swirl injector. They deeply investigated geometric parameters effect on the spray cone angle. They employed experimental and numerical methods and the spray cone angle significantly influences by the divergent angle and the swirl chamber diameter. They detected increasing the divergent angle produces a smaller spray cone angle.

Kim et al. (2013), investigated spray and combustion characteristics for direct injection compression ignition engine. The macroscopic spray visualization and optical engine system were used for their experimental studies. They detected that the gasoline spray was shorter liquid penetration length compared with the diesel spray under the non-evaporation condition and the spray angle was larger than diesel spray.

Chen et al. (2013), carried out numerically and experimentally study for common rail fuel injection system. The spray and atomization characteristics were investigated with diesel and alternative fuels for single hole injector. They measured droplet diameters and particle size distributions. They observed that alternative fuels show closer droplet size and spray penetration with both smaller than diesel. Their results showed that increasing injection pressure is effective at reducing the droplet size.

Raju and Rao (2015), used CONVERGE CFD code in their study for investigated to fuel injection pressure and spray cone angle effects on direct injection engine performance. Their simulation results showed that the spray cone angle has a significant effect on engine performance and emissions. They detected small cone

angle values are better for combustion and emission performance in the engine.

Kannaiyan and Sadr (2014), experimentally investigated alternative fuels spray characteristics for aviation. Their experimental study results showed that the fuel spray characteristics physical properties affect the regions close to the nozzle exit at the higher injection pressure. They used two different fuels as one is Jet A-1 and the second one is GTL fuels. They obtained the effective spray cone angles for both fuels at different pressure conditions.

Rashad et al. (2016), carried out an experimental study for pressure swirl atomizers and investigated geometric parameters on spray characteristics. They measured the spray cone angle via a high-speed camera for different geometric configurations and injection pressures. They observed that the spray cone angle continuously decreases with the increase of swirl chamber orifice diameters and the Sauter mean diameter.

The development of modeling software, the results obtained from these software's and the reasonable approximation of experimental results have been experienced in many studies in the literature (Patterson and Reitz, 1998; Watanabe et al., 2007; Mitroglou et al., 2006; Skogsberg et al., 2005; Battistoni and Grimaldi, 2012; Park et al., 2009; Liu et al., 2013; Kim et al., 2013; Raju and Rao, 2015). Numerous increasing number of approaches are employed for in-cylinder combustion and flow, the two most important criteria determining the accuracy of modeling software. The commonly used combustion models for in-cylinder is G-equation, Extended/Coherent Flame Model/3-Zone (E/CFM/3Z), Magnusson's Eddy Break-up, Ricardo Two-Zone Flamelet Model. In addition, k- $\epsilon$ , k- $\epsilon$  RNG, Large Eddy Simulation (LES), Reynolds Averaged Navier Stokes (RANS) models are also employed as turbulence models. The G-equation/k- $\epsilon$  RNG pair as a model of combustion and turbulence gives results closer to the experimental results in SI engines. In the case of CI engines, the ECFM-3Z/LES pair represents better in-cylinder combustion (Mitroglou et al., 2006; Skogsberg et al., 2005; Battistoni and Grimaldi, 2012; Raju and Rao, 2015).

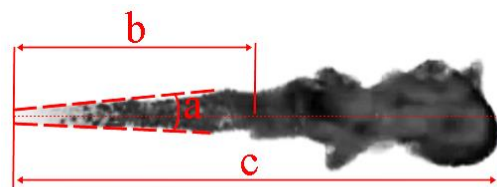
In this study, the effects of spray cone angle change on combustion and performance, which is one of the spray parameters for kerosene use in a direct injection compression ignition engine, were investigated by numerical analysis by modeling the in-cylinder combustion. The optimum spray cone angle was determined by CFD analysis. For this purpose, in-cylinder combustion was modeled in Star-CD software and effects of spray cone angle change on kerosene fuel were investigated. As a result of the analysis of a certain engine operating condition; optimum spray cone angle has been determined for performance and emissions. In addition, the effects of in-cylinder spray development

and effects were evaluated. For the CFD model, 5 different angles between 5° and 25° were examined. In numerical modeling, speed, compression ratio, and excess air coefficient were kept constant.

## SPRAY THEORY AND CFD MODEL

In compression-ignition engines, the engine speed and power are controlled by the fuel injected into the cylinder during the cycle. In the engines, since fuel particles are not burned at the same time and burning period spreads a short time of the cycle, it is desired to have different fuel droplet sizes. This reduces pressure pulses acting on the piston head and ensures better engine performance. It is desirable to have the constant spray time at all engine speeds. To achieve this, the spray pressure is changed to increase with the square of the engine speed. The spraying processes are carried out in two parts as pre-spraying and the main spraying to increase the efficiency of the spray, reduce the ignition delay time and reduce the formation of soot.

Three main parameters are employed to define the spray geometrically sent from the injector to the combustion chamber. These parameters are break-up length, penetration length and spray cone angle (Fig. 1). The injector pressure, injector internal geometry, the geometric structure of the spray, size of the particles, velocities, turbulence movements in the combustion chamber, the temperature of the air in the combustion chamber and the pressure determine the behavior of the spray in the combustion chamber. These parameters then directly affect the emission formation in the combustion process. The different fuel particle size and the gravitational force between the fuel particles are important for the spray behavior in-cylinder.



**a: Spray Cone Angle**  
**b: Break-Up Length**  
**c: Spray Penetration Length**

**Figure 1.** Parametric definitions of a spray.

The spray core is divided five zones which are ultra-rich, rich combustible, stoichiometric, lean combustible and ultra-lean. Even though the spray is divided into five regions, it is possible to observe different air-fuel mixture ratios in each area on the spray geometry after the spray scattering in the cylinder Fig. 2. Spray cone angle affects the droplet distribution after atomization. Two important characterization parameters for spray development are spray cone angle and ignition delay. In the literature, it is possible to see many equations related

to these two parameters (Patterson and Reitz, 1998; Wakuri, et al. 1960; Dent, 1971; Hiroyasu and Arai, 1990). Ignition delay is a powerful function of time, while the spray angle is a powerful function of fuel structure and injector pressure.

In this study, a cylinder of a direct injection commercial compression-ignition engine was examined. The technical specifications of the test engine are listed in Table 1. The injection system is formed in a way that the fuel cylinder can be sprayed directly from 10 different points. The engine piston has an omega type combustion chamber.

**Table 1.** Parametric definitions of a spray.

Number of cylinder	1
Cylinder volume, cc	1991
Cylinder diameter, m	0.130
Stroke length, m	0.150
Compression ratio	17:1
Number of valve	4

The geometry of the single cylinder for the engine is shown in Figure 3. Since only the closed cycle is analyzed, the geometry has been created by considering the range in which the valves are closed ( $-40^\circ$  CAD before top dead center (BTDC) to  $80^\circ$  CAD after top dead center (ATDC)). The solid model of the cylinder and related components of the engine has been formed by using the dimensions obtained with coordinate-measuring machine (CMM) device.

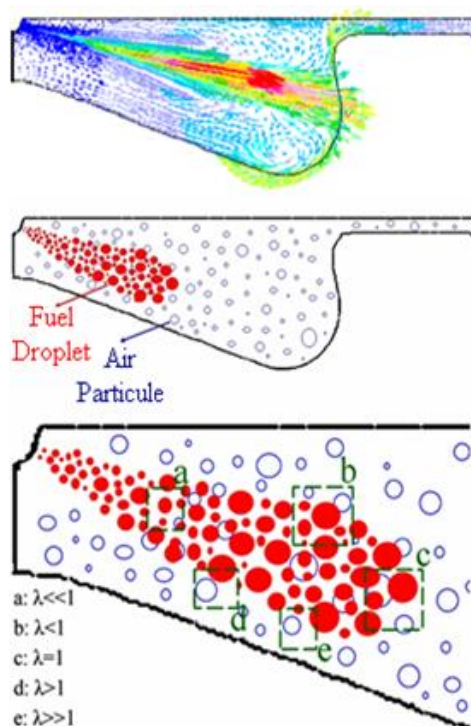


**Figure 2.** Spray and atomization profile.

The modeled geometry also includes the injector nozzle, which is centrally located on the cylinder head. The other parts of the model are consist of the cylinder liner and the piston. The cylinder liner surface is extended as the piston moves over time in the 3-D dynamic combustion model.

The Star-CD software has been used for in-cylinder combustion model. For the analysis of CFD, a 2-dimensional mesh was created for the surfaces surrounding the entire model volume then a 3-dimensional mesh was formed for the volume closed with surfaces. Thus, the whole model volume is filled with the mesh structure. The omega combustion chamber area is defined as moving zones on the mesh so as to move depending on engine cycle times.

In the analysis performed, the engine speed was kept constant at 1300 rpm, compression ratio 17:1 and excess air coefficient at 1.7 and optimum spray cone angle was determined under these conditions. The in-cylinder EGR ratio is defined as 5% of the known value for the engine (CD-Adapco Star-CD, 2016).

Kerosene was defined as the fuel used in the 3-D CFD model, the properties and sub-species of the kerosene were defined in the software by Chemkin via 0-D pathway. Kerosene is a petroleum derivative that is generally used in industry and aviation industry. Kerosene is obtained by very fine distillation of the petroleum at 423 K to 543 K and the flash point of kerosene is between 310 K and 340 K. Kerosene carbon chains are contain between 10 and 16 carbon atoms per molecule. It is used in aircraft engines as commercial aviation fuel because of its properties and low viscosity (Mang et al., 2007). It is suitable for use in environments with very low temperature because of the freezing point ( $\sim 220$ K). In addition to its flammability, it keeps the liquid form at low temperatures and is mixed into 20% of the fuel used in aircraft (Mang et al., 2007).

Kerosene ignites more difficult than gasoline but gives more heat energy than gasoline. Kerosene consumption is equivalent to about 1.2 million barrels per day for the whole over the World and its lower heating value is 43.1 MJ/kg is similar to that of diesel fuel (Mang et al., 2007). Kerosene fuel is also known as-JET-A1 fuel in the aviation sector and mixed species such as JET-B, JP-4, JP-5, JP-7 and JP-8 are also employed (Mang et al., 2007). The reason for using kerosene in this study is that many direct injection engines are used in aircraft in aviation sector and kerosene-natural gas usage is widespread in newly developed dual fuel engines.

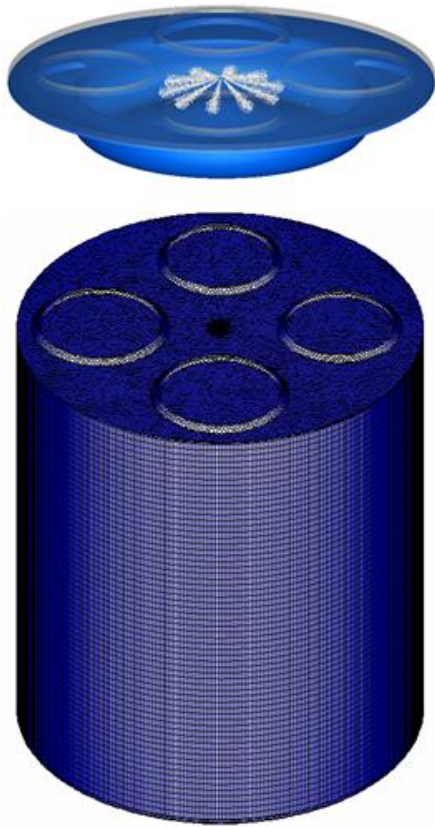


**Figure 3.** Geometry of the single cylinder.

Versatile combustion models are available for the modeling of the in-cylinder. In this study, ECFM-3Z/Compression combustion model developed for modeling of combustion in compression-ignition engines was used. The ECFM-3Z (Extended Coherent Flame Model-3 Zones) combustion model (CD-Adapco, 2016) is a suitable analyze model for both spark-ignition (direct injection) and compression-ignition engines. The basic approach in this combustion model is to divide the solution volume into three regions to calculate local layering. In the section of burnt gases in the mixture zone, the improved model of post-flame chemistry is solved. In the section of unburned gases, the standard ECFM combustion model is solved by the addition of a self-ignition model. The “3Z” term for mixture model represents three mixing regions. These mixing regions are unmixed fuel zone, unmixed air-residual gas zone and mixed gas region (CD-Adapco, 2016). In the ECFM-3Z model; flame propagation and post-flame emissions are calculated by reference to gases in the mixture zone. Model contains reaction sets in burnt gas such as; “Fuel Oxidation Chemistry”, “Dissociation”, “Root Formation Chemistry”, “CO $\rightleftharpoons$ CO<sub>2</sub> Kinetics Chemistry”, “NO Chemistry”, “Soot Chemistry” and the structure of these chemistry sets is utilized in the analysis (CD-Adapco CD-Meth., 2016). This combustion model consists of two steps. In the first step, the delay time is modeled. In the second step, the actual spread of the flame surface within the average gases is taken into account. The mixture region is turbulent, the gases in other regions are the result of the molecular

mixture-diffusion and where combustion occurs (CD-Adapco, 2016).

The turbulence model has been proposed for internal combustion engines and k- $\epsilon$  RNG turbulence model, which is widely used in literature (CD-Adapco, 2016), and Angelberger wall functions as wall function were employed. For the in-cylinder surfaces, the general temperature definitions specified in the literature are employed. The combustion peak zone (550 K), the piston peak zone (600 K), and the cylinder wall zone (550K) were defined in the 3D model (Mahle GmbH, 2012).

Monotone Advection Reconstruction Scheme (MARS) method was used for the dissociation of equations related to flow area, temperature distribution and turbulence. The Pressure Implicit Splitting of Operator (PISO) algorithm is selected for the velocity-pressure pair. The CFD model parameters defined for the kerosene in the analyzes are listed in Table 2.

The spray atomization model Huh (1991), droplet break-up model Reitz and Diwakar (1986), droplet behavior Bai (Bai and Gosman, 1995) were selected in the model. Spray Huh’s model is based on the premise, supported by order-of-magnitude estimates, that the two most important mechanisms in spray atomization are the gas inertia and the internal turbulence stresses generated in the nozzle. According to Reitz and Diwakar model, droplet break-up due to aerodynamic forces defined in two ways. The first one is Bag break-up, in which the non-uniform pressure field around the droplet causes it to expand in the low-pressure wake region and eventually disintegrate when surface tension forces are overcome (Reitz and Diwakar, 1986). The second one is stripping break-up, a process in which liquid is sheared or stripped from the droplet surface. In each case, theoretical studies have provided a criterion for the onset of break-up and concurrently an estimate of the stable droplet diameter and the characteristic time scale of the break-up process (Reitz and Diwakar, 1986).

**Table 2.** CFD model parameters.

Turbulence intensity	0.1
Length scale	0.001
Penetration length, m	0.025
Injection temperature, K	320
Injection pressure, bar	950
Spray umbrella angle, °	126
Hole diameter, m	0.0004
Nozzle L/D	6
Molecular viscosity	Sutherland
Break-up model	Reitz and Diwakar
Spray atomization model	Huh
Droplet behavior	Bai

In time-based analysis; 0.05° CAD resolution time step between -40° CAD before top dead center (BTDC) to 80° CAD after top dead center (ATDC), 0.025° CAD resolution time step between -20° CAD BTDC to -10° CAD BTDC and 0.010° CAD resolution time step between -10° CAD BTDC and 80° CAD ATDC were defined. All obtained solution parameters (pressure, temperature, emissions, etc.) are recorded in the result file.

While the full cycle interval was -360° CAD BTDC to 360° CAD ATDC, the closed cycle analysis was performed in the range of -40° CAD BTDC to 80° CAD AFTDC. In the specified cycle, the crankshaft angle of the spray injection advance is -5° CAD BTDC and at the end of the compression time, the piston reaches the top dead center (TDC) at 0° CAD. The spray cone angle was changed between 5°-25° CAD by 5° CAD interval and analyzes were made for 5 different spray cone angles.

In order to ensure the mesh independent solution, before the analysis of the spray cone angle effects, a cold flow analysis was run for various number of meshes. The adequacy of the mesh elements forming and the correct functioning were checked. In addition, the flow structure is controlled to be within the known expectations. Table 3 shows the number meshes vs. maximum kinetic energy and maximum turbulent kinetic energy for the cold flow. Furthermore, a mesh structure operation was carried out on the spray geometry and the injector area in order to fully evaluate the spray efficiency. The mesh structure sensitivity on the spray was adjusted to the extent allowed by the available computer infrastructure (Fig. 4). When the total number of mesh elements reached 3.7 million, it was seen that maximum kinetic energy and maximum turbulent kinetic energy were the inside of the cylinder no longer changed, and this 3-D mesh structure shown in Figure 3 was employed in all analyzes.

**Table 3.** The variance of maximum kinetic energy and maximum turbulent kinetic energy by mesh numbers.

Mesh numbers	Maximum kinetic energy (m <sup>2</sup> /s <sup>2</sup> )	Maximum turbulent kinetic energy (m <sup>2</sup> /s <sup>2</sup> )
607.706	857	40
821.667	894	39
1.215.689	925	38
1.736.929	948	36
2.499.855	963	33
3.120.176	964	32
3.707.141	964	32

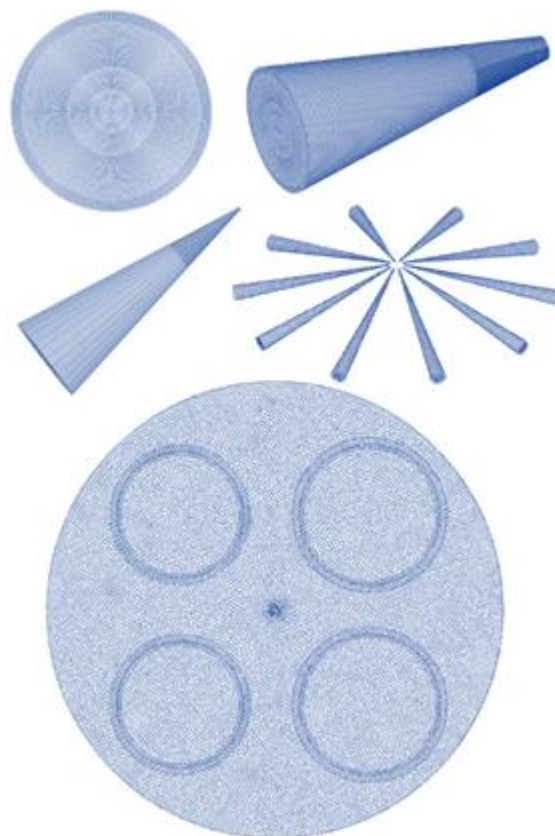


**Figure 4.** CFD domain and mesh views.

In order to validate the CFD model, in addition to mesh independency analyses, the CFD model was run for diesel fuel at the maximum torque conditions given in the engine catalogue. This torque in the CFD model was calculated and 2.12% higher than the catalogue value. This small difference is acceptable since all test losses are measurable and not embedded into the 3-D engine model. After verifying the CFD model, the kerosene usage analyses were run for five different spray cone angles.

After making all the necessary definitions for the CFD model, five spray cone angles were analyzed and solutions were obtained. Using the obtained solutions, the result graphs for the calculated parameters are created and evaluated below.

## RESULTS

The CFD analyses were performed for the closed cycle after the creation of the geometry and mesh structures, the definition of the boundary-initial conditions and the approaches to be used in modeling.

In order to examine the effects of the spray cone angle and to find the optimum cone angle value for the specified operating conditions, analyses were made for each spray cone angle using the 3D CFD model in the direct injection engine. In addition, the engine characteristics were calculated and in-cylinder combustion and emission formation were visualized.

The change of in-cylinder pressure according to CAD for the five spray cone angles examined is shown in Figure 5. The highest in-cylinder pressure value was observed at 20° spray cone angle (SCA). Increased in-cylinder pressure with compression for all spray cone angles, rises rapidly from the end of the ignition delay and reaches its maximum after a bit the TDC and then changes to the trend of decrease. As the spray cone angle increased, the pressure inside the cylinder raised and it showed a downward trend after 20° SCA. When the maximum pressure values are examined, the in-cylinder pressure at 20° SCA is 15.8% higher than 5° SCA. Furthermore, the maximum value of the in-cylinder pressure at 25° SCA is 6.1% lower than 20° SCA. As the spray cone angle increases, the progression of the droplets in the gas is reduced by exhibiting the solid behavior and earlier break up occurs in-cylinder. More high-temperature air particles penetrate into the spray. The air particle collides with more fuel particles. As a result, more fuel particles react with air then so the pressure and temperature increase.

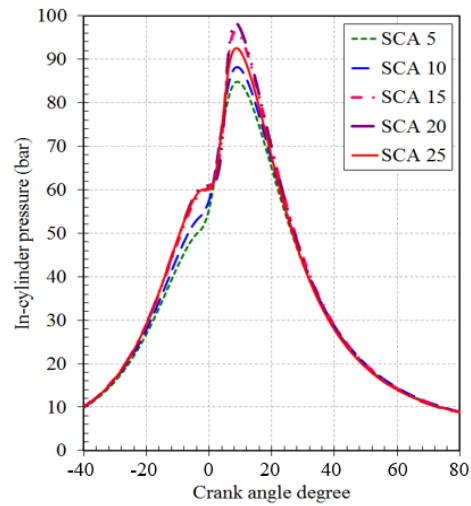


Figure 5. In-cylinder pressure.

The average temperature in-cylinder curves are shown in Figure 6. The increased in-cylinder temperature at the time of compression rises up rapidly from the end of the ignition delay after fuel spray injection and gradually decreases with a lower slope after reaching the peak. The temperature in-cylinder increases to 5°-20° SCA while the highest temperature in-cylinder rises up from 1620 to 1720 K. As the spray cone angle increases, more fuel molecules collide with the air molecule and form a combustion reaction. This leads to more heat energy in the cylinder and an increase the temperature. When the spray cone angle was 25°, the temperature exhibited a downward trend. The higher cone angle causes the surfaces to get wet by the fuel molecules, to increase the cooling tendency on the fuel molecules. As a result of this, the fuel molecules react early and lesser and reduce the temperature inside the cylinder.

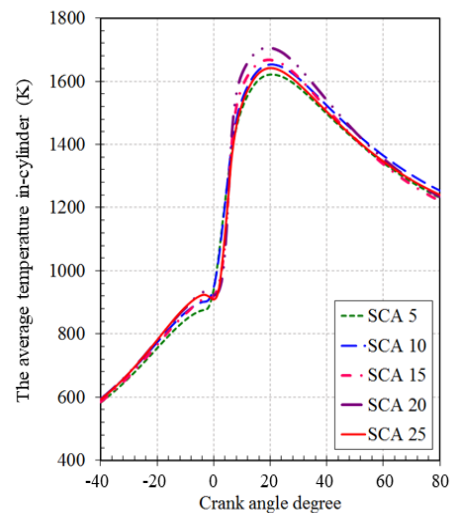


Figure 6. The average temperature in-cylinder.

When dissipation curves in Figure 7 are examined for spray cone angles, overall dissipation showed a declining trend. When the maximum dissipation curves are examined, 20° SCA dissipation is 43.5% lower than 5° SCA. As the cone angle decreases, less fuel will react and the amount of energy utilization will decrease. As can be seen from the areas in the graph, the decrease in the spray cone angle increases the time for dissipation.

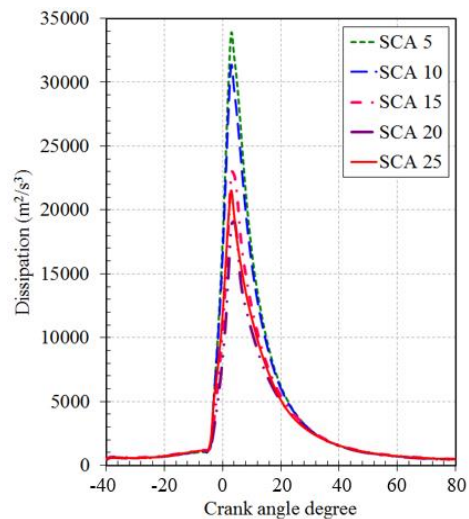
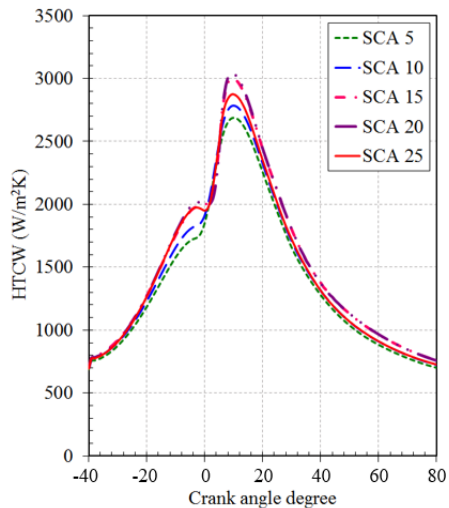


Figure 7. Dissipation.

The heat transfer coefficient on wall (HTCW) curves are showed in Figure 8. As the spray cone angle increases, it is seen that the heat transfer from the cylinder walls rises up. The HTCW values climb from 2688 W/m²K to 3037 W/m²K when the spray cone angle increases. This is because more fuel molecules collide with more air molecules, resulting in more heat energy in the cylinder.



**Figure 8.** Dissipation.

The indicated power and the indicated mean effective pressure (IMEP) were calculated for all spray cone angles. The performance parameters are shown in Figure 9 with a bar graph. When the spray cone angles are examined for IMEP, at 20° SCA were calculated as 4.06% and 3.41% higher than 5° SCA and 25° SCA, respectively. For indicated power, at 20° SCA were calculated as 7.98% and 6.72% higher than 5° SCA and 25° SCA, respectively. Increasing the distance between the particles forming the spray is possible with the increase of the spray cone angle. As a result of such an increase, the spray break-up length is shortened. In this case, the air molecules influence the spray geometry over more contact areas, causing more fuel molecules to be cracked into the sub-species. This allows more fuel particles to enter the combustion reaction. At very small spray cone angles, the spray-forming liquid particles will exhibit solid behavior and will have less contact with air. As a result, the fuel molecules will not be able to pass to the gas phase and the chemical energy of the fuel molecules will not be sufficiently utilized.

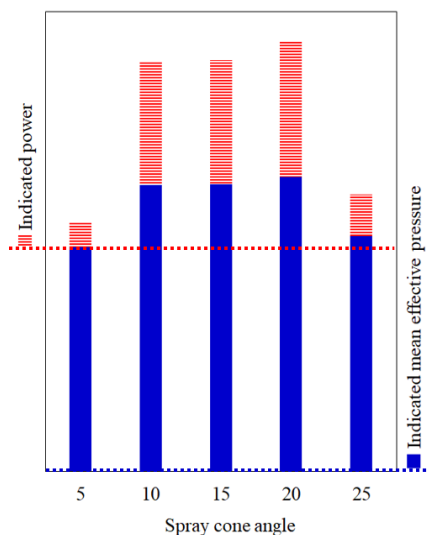


**Figure 9.** Indicated power - IMEP.

The fuel in the burnt gases curves are shown in Figure 10. The curves in the graph support the behavior of SCA curves for in-cylinder temperature, dissipation, in-cylinder pressure, and indicated power-IMEP graphs. As the SCA increases, the combustion reactions are spread over more areas in-cylinder and the unburned fuel observation takes place over a longer period of time. Furthermore, there is a decrease in the amount of fuel sent from the cylinder to the exhaust line without reacting when the SCA increases. In addition, if the spray angle is too small, the fuel jet will be in a very rich mixing zone and the combustion reaction will start very rapidly on the outer surface of the spray, and then a rapid decrease will be observed and the dissipation graph strongly supports this situation. It is seen that on the graph when the SCA is increased by 5 times, the amount of unburned fuel in the burned gases decreases by 50% on average. The fact that the fuel cannot be fully burned means that it cannot fully utilize the energy generated by the mass and the lower heating value of the fuel. In this case, the average pressure on the piston head and the net work area from the engine decrease. The fuel, which cannot be fully burned, also leads to the formation of CO, HC components, which are incomplete combustion products.

The curves of CO<sub>2</sub>, CO, OH, NO<sub>x</sub> and soot are shown in Figure 11, Figure 12, Figure 13, Figure 14 and Figure 15 respectively. Generally for all spray cone angles: the CO<sub>2</sub> contained in the air initially received in the cylinder remains constant at the time of compression and climbs exponentially at the end of the ignition delay. As the spray cone angle increases, the number of reactions by the fuel molecules and the air molecule rises up. The contact of more fuel droplet surface area with air molecules increases complete combustion formation and consequently increases the amount of CO<sub>2</sub>. The maximum CO<sub>2</sub> formation occurs when the spray cone angle is 20° SCA. When the cone angle continues to increase, CO<sub>2</sub> formation decreases due to the cooling of the fuel molecules after wide spread in the cylinder. For CO<sub>2</sub> formation, at 20° SCA is 24.3% higher than 5° SCA.

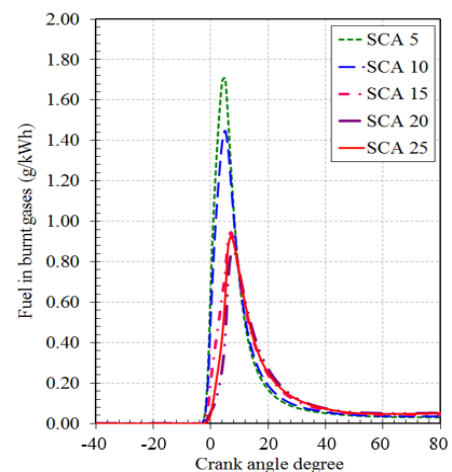


**Figure 10.** Fuel in burnt gases.

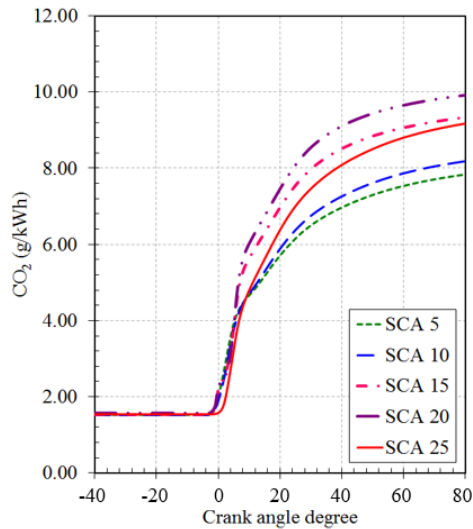


**Figure 11.** CO<sub>2</sub> emission.

The amount of CO curves in-cylinder at Figure 12 show an inverse behavior to the amount of CO<sub>2</sub>. By the end of the compression time, the CO occurrences started to be seen in the cylinder. The CO formations accelerate as the spray cone angle increases. At narrower spray cone angles, the CO formations exhibit a more stable behavior and spread over a long time in the cylinder. The amount of CO which rises up rapidly with the increase of the spray angle, then reacts with the free O<sub>2</sub> molecules and turns into CO<sub>2</sub> as the combustion continues in the cylinder. Therefore, the amount of CO decreases. It is seen that the lowest CO amount is observed when the spray angle is 20° SCA and this behavior is also supported by the CO<sub>2</sub> graph. At 20° SCA, CO formation is 7.8% lower than 5° SCA and 17.2% lower than 25° SCA.

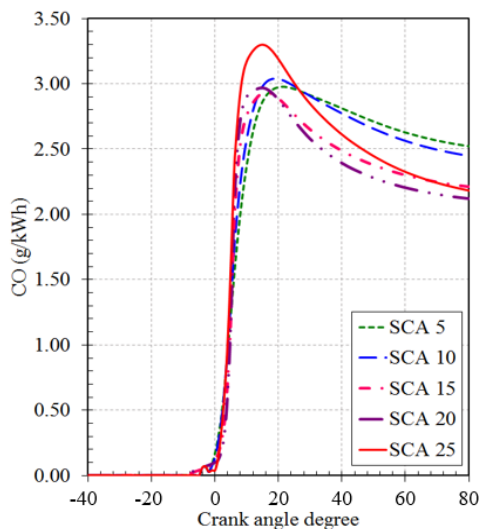


**Figure 12.** CO emission.

The temperatures in-cylinder greater than 1000 K, dissociated reactions during the combustion process will result in additional species such as OH, CH, NO, H, O etc. for internal combustion engines. Some radical species, such as OH, emit radiation at certain wavelengths and OH chemiluminescence has some advantages for detecting heat release in diffusion flames. Thus, OH provides information about the conditions in the chemiluminescence reaction zone and the flame propagation. Therefore, it is important to examine the OH behavior to evaluate the effects of spray cone angle change. As can be seen from Figure 13, the formation of OH rises up like the spray cone angle increases. Rapidly rising OH formation during the combustion period after ignition delay; provides information on the flame formation, flame propagation and location of the flame. The OH formation at 25° SCA is 42.8% higher than 5° SCA.

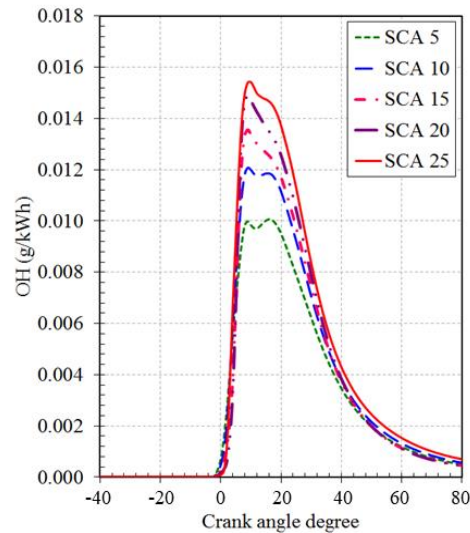


**Figure 13.** OH emission.

The free N<sub>2</sub> and O<sub>2</sub> molecules in the cylinder react with the increase of the temperature in the combustion chamber to form structures such as NO, NO<sub>2</sub>, NO<sub>3</sub>. NO<sub>x</sub> formations are described according to Zel'dovich mechanisms (Miller et al., 1998). These mechanisms consist of the combinations of O ions and free N<sub>2</sub> molecules, O<sub>2</sub> molecules with N ions and the free OH ions and N ions. As high temperatures are reached in the cylinder, the molecules are exposed to thermal dissociation such as O, OH, H<sub>2</sub>, N, etc. These dissociated sub-molecules and ions reunify to causing NO<sub>x</sub> formation. When the NO<sub>x</sub> graph in Figure 14 is examined, the increased spray cone angle causes more fuel molecules to react with the air molecules, resulting in more chain or branched chain combustion reactions and increased temperature in the cylinder. As a result, increased in-cylinder temperature rises up thermal dissociation and NO<sub>x</sub> formation. The NO<sub>x</sub> formation for 25° SCA is higher 51.2% than 5° SCA. On the other hand, NO<sub>x</sub> formation for 20° SCA is 19.2% lower than 25° SCA.

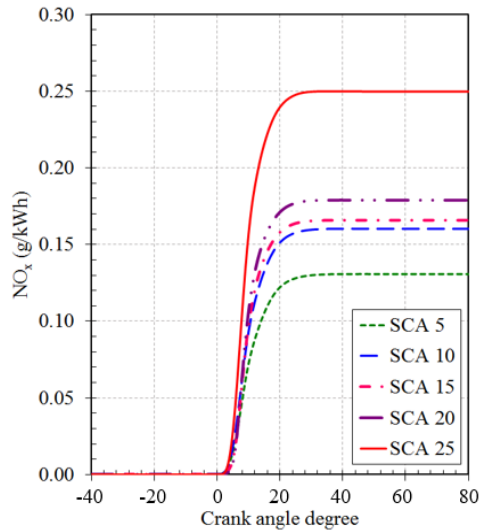


**Figure 14.** NO<sub>x</sub> emission.

The NO<sub>x</sub> formation behaviors supporting curves are possible to be seen in the soot formation graph (Figure 15). The formation of soot occurs as a result of the inability to fully oxidized the fuel molecules. Soot is formed in regions where the temperature in the cylinder cannot reach a sufficient level. As the spray cone angle decreases, less fuel droplet surface will come into contact with air, oxidation formation will be reduced and the fuel molecule will not be fully oxidized and will be passed to cooling phase. In short, this situation means the formation of soot. At narrower spray cone angles, the fuel droplet injected from the injector collides to fewer air molecules and completes the combustion reactions without fully reacting and it turns into soot. The reaction of the carbon molecules in the fuel with the maximum number of air molecules leads to a decrease in the formation of soot.

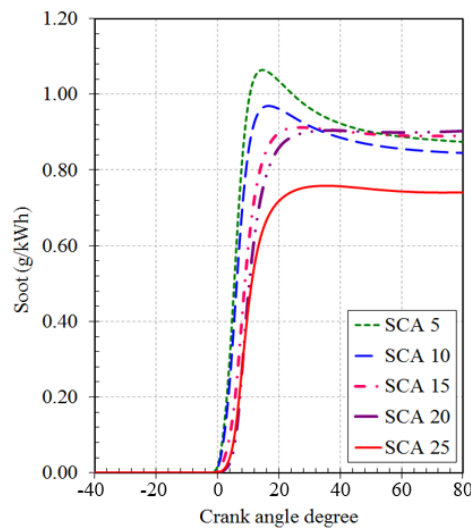


**Figure 15.** Soot emission.

As the spray cone angle increases, the carbon and hydrogen molecules in the fuel react more with the air molecules. As a result, the formation of CO<sub>2</sub>, CO, OH, H<sub>2</sub>O, NO, NO<sub>2</sub>, NO<sub>x</sub> increases while the formation of soot decreases. Multiple injection strategies are applied to internal combustion engines to minimize soot formation. With this strategy, the fuel molecule is re-reacted with a second injection in the period of conversion to soot, thus preventing the formation of soot (Heywood, 1988). For soot formation, at 25° SCA is 40.7% lower than 5° SCA. In addition, soot formation at 20° SCA is 24.8% lower than 5° SCA.

The effects of the droplet velocities are shown in Figure 16, Figure 17 and Figure 18 with the OH, NO<sub>x</sub> and soot curves. The attraction force of the fuel droplets is reduced. Because of the increase in spray angle, the fuel molecules move away from each other and shortens the break-up length. As a result, the air molecules entering into the spray slow down the fuel molecules with both momentum transfer and react, causing their size to shrink and break down. The examination of the variations by droplet velocities provide us with information about the time taken for the molecular formations and the angle of the molecular formation zones within the cylinder. When the OH graphic is examined, the fuel particle coming out of the injector starts to move with high acceleration due to the momentum gained in the injector. Particularly, after the outer surface of the spray geometry directly collides the hot air molecules at the injector outlet, the formation of OH reaches the maximum level shortly after the injection process. As the spray cone angle increases, a higher amount of OH is formed as expected after more molecules are rapidly contacted with air. Reduction of the spray cone angle causes the formation of OH in the cylinder for a long time. Because it takes time for all the fuel molecules that form the spray to react.

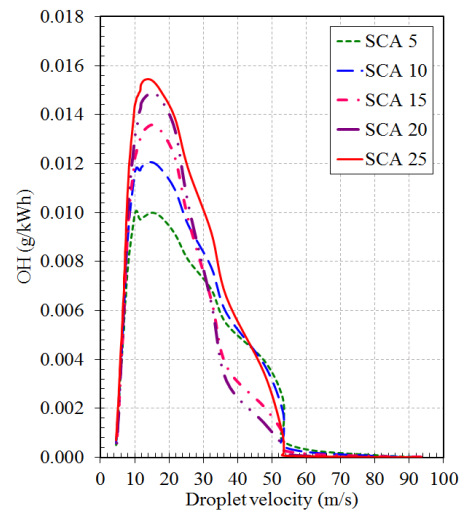


**Figure 16.** OH-droplet velocity.

When the  $\text{NO}_x$  curves are examined, it is seen that the fuel molecules leaving the injector react very quickly with air as the spray cone angle increases. As a result, the ignition delay time is shortened and the temperature rises rapidly with the start of combustion. Therefore,  $\text{NO}_x$  formation occurs faster than narrow spray angles. As can be seen from the graph, the formation of soot increases as the spray cone angle decreases. The fuel particles, which retain their shape for longer periods at narrow spray cone angles, enter a complete reaction with air in a long process. In the meantime, many fuel molecules cannot fully oxidize and they turn into soot. Due to a long time of the full reaction at narrow spray cone angles, most of the fuel droplets turn into soot and the literature supports the results (Mitroglou, 2006).

The ignition delay is terminated just before the TDC and flame formation is observed. Temperature (Figure 19), OH (Figure 20),  $\text{NO}_x$  (Figure 21) and soot (Figure 22) formations at different spray cone angles in  $-2^\circ$  CAD BTDC to  $12^\circ$  CAD AFTDC range are shown in the contour graphs. As the spray angle increases, a high temperature zone is observed in the omega combustion chamber near the top surface. When the spray cone angle increases, the fuel molecules reach everywhere and react with air molecules in the cylinder then the higher temperature areas grown in the cylinder. It is possible to see that OH formations are more pronounced initially as the spray cone angle decreases in the OH contour graph (Fig. 20) and also supports OH curves in Fig. 13. The OH contour graph also supports the temperature contour graph, too.

As a matter of fact, OH formation areas are observed in the part where the temperature is high in the cylinder. As the time progresses and the spray cone angle increases, OH zones are observed in the cylinder.  $\text{NO}_x$  contour graphs show  $\text{NO}_x$  occurrences in high temperature areas and both the  $\text{NO}_x$  curves (Fig. 14) and the temperature contour graph (Fig. 19) support this situation.  $\text{NO}_x$  formations are observed in omega combustion chamber due to high temperature in the regions close to the piston top surface. It is also important to note that the narrowing of the area makes the temperature between the piston top surface and cylinder head and the  $\text{NO}_x$  formation is observed in this region.

The soot contour graph supports the  $\text{NO}_x$  contour graph and soot curves. As the spray cone angle decreases, soot formation is observed towards the center of the omega combustion chamber. The comparison contour graph for temperature,  $\text{NO}_x$ , and soot is shown in Figure 23 at the

same CAD. In the contour chart, the region of “a”, where the temperature is high, there are similar “b” regions where the  $\text{NO}_x$  formation is high. On the other hand, the “c” region where the temperature is low is the region with the highest amount of soot formation. The contour graphs show that the amount of soot increases and the  $\text{NO}_x$  amount decreases with the cone angle narrows.

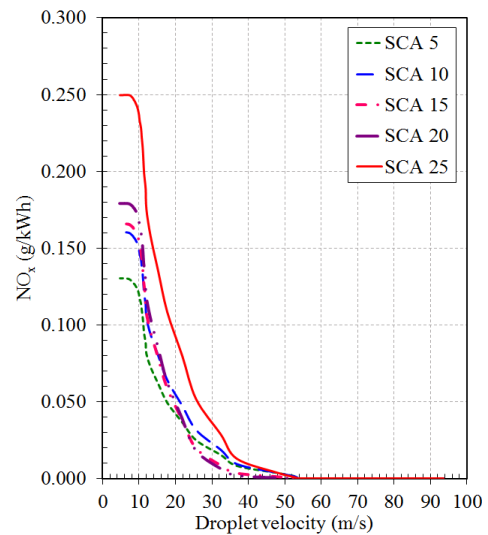


Figure 17.  $\text{NO}_x$ -droplet velocity.

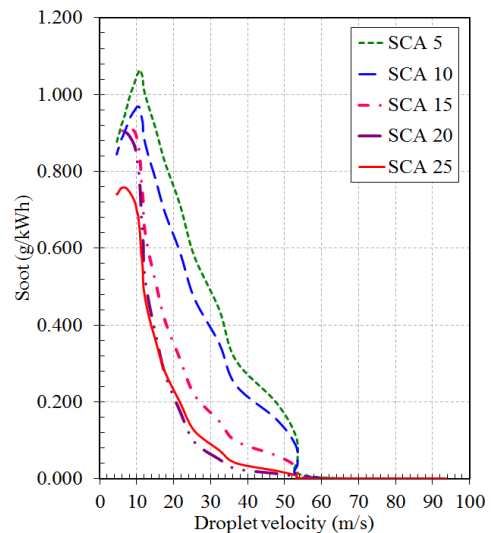


Figure 18. Soot-droplet velocity.

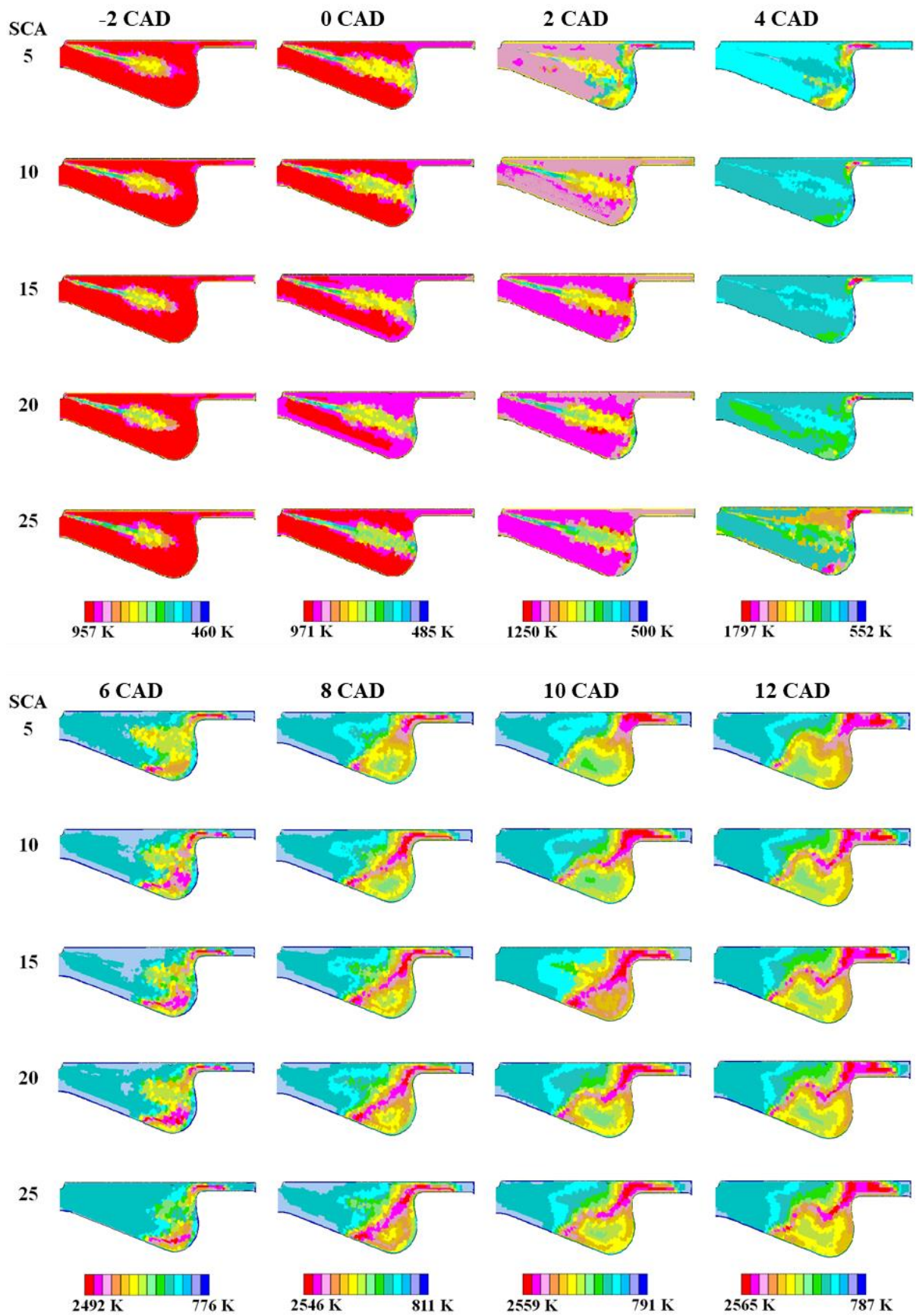


Figure 19. In-cylinder temperature contours.

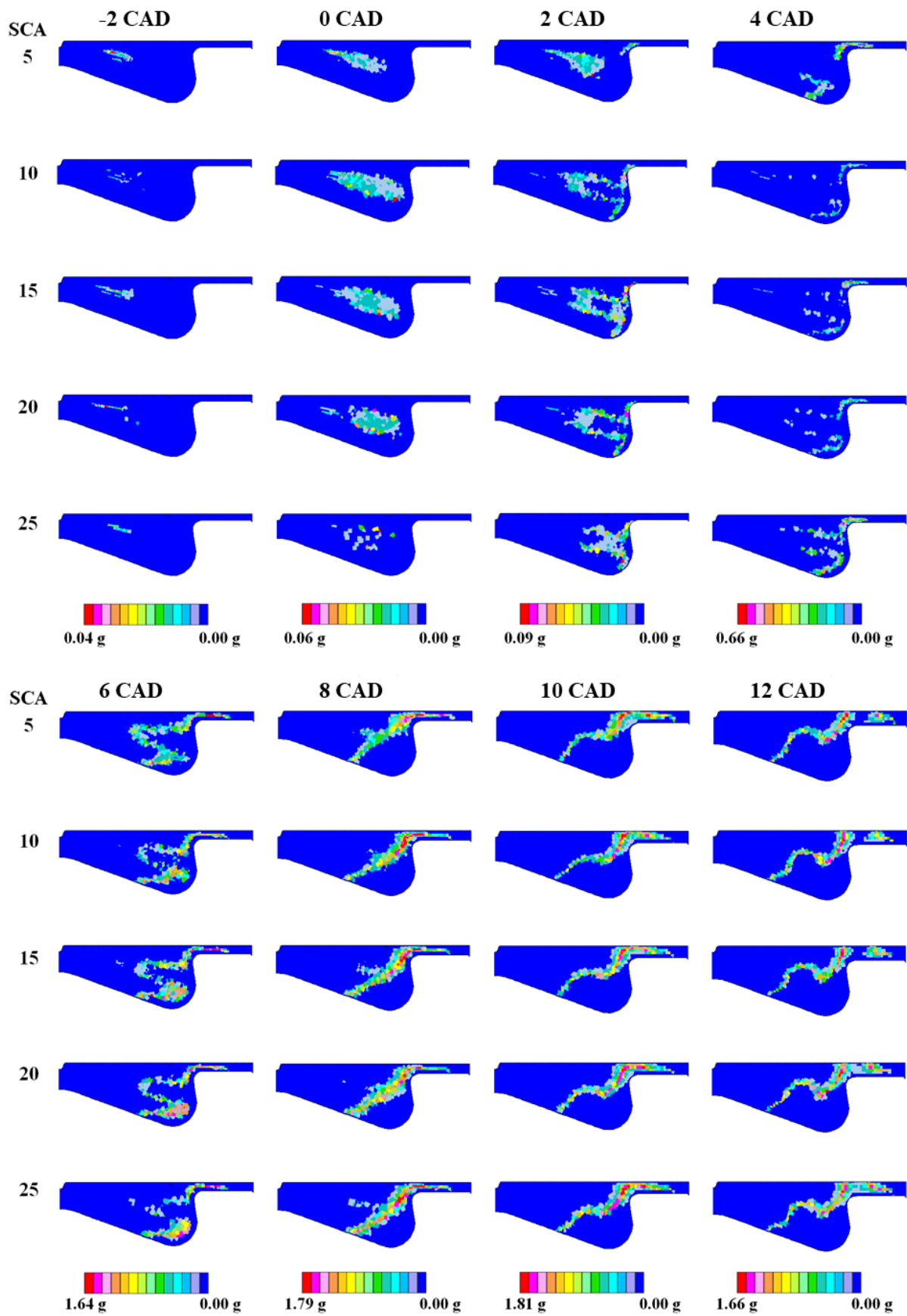


Figure 20. OH contours.

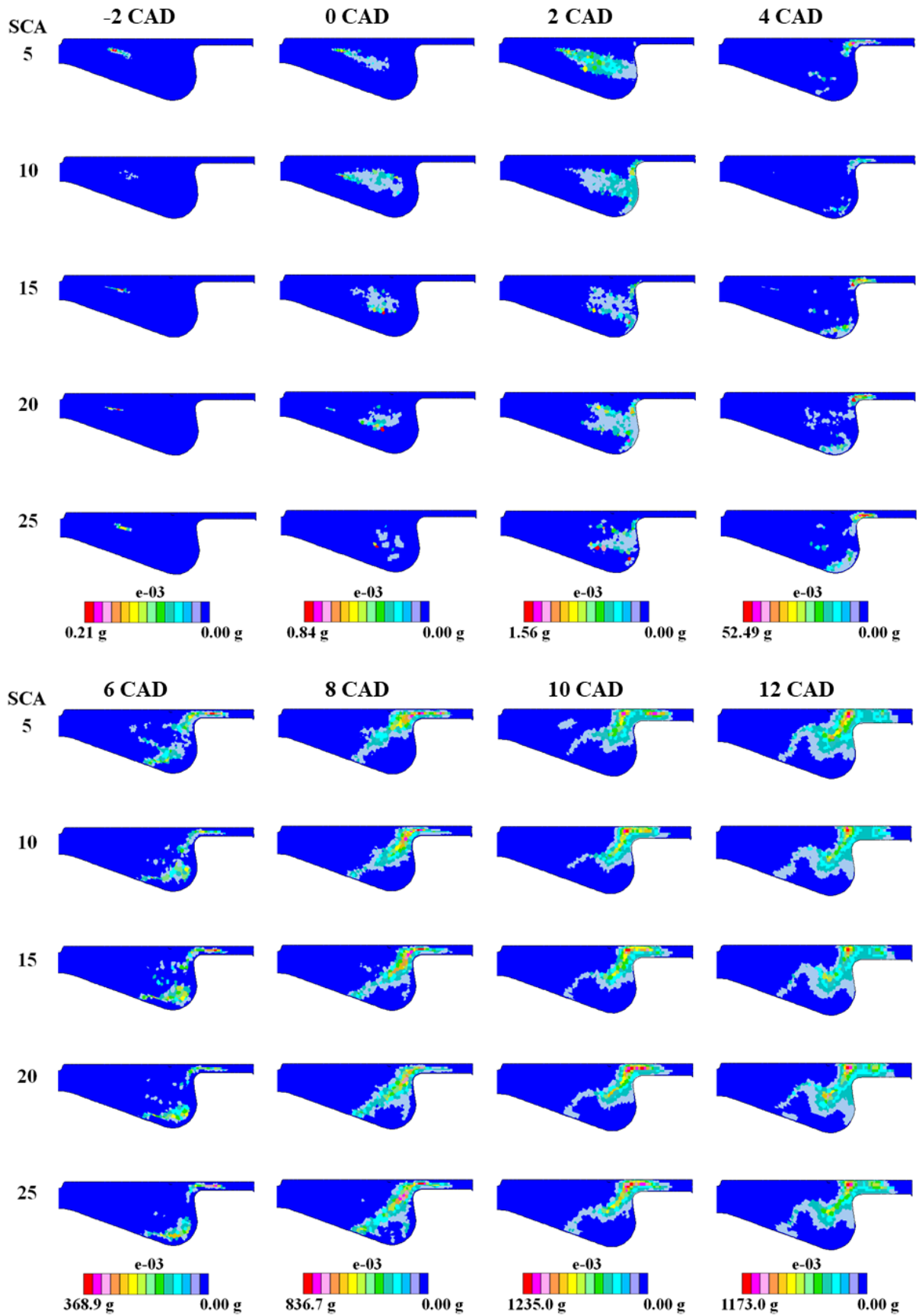


Figure 21. NO<sub>x</sub> contours.

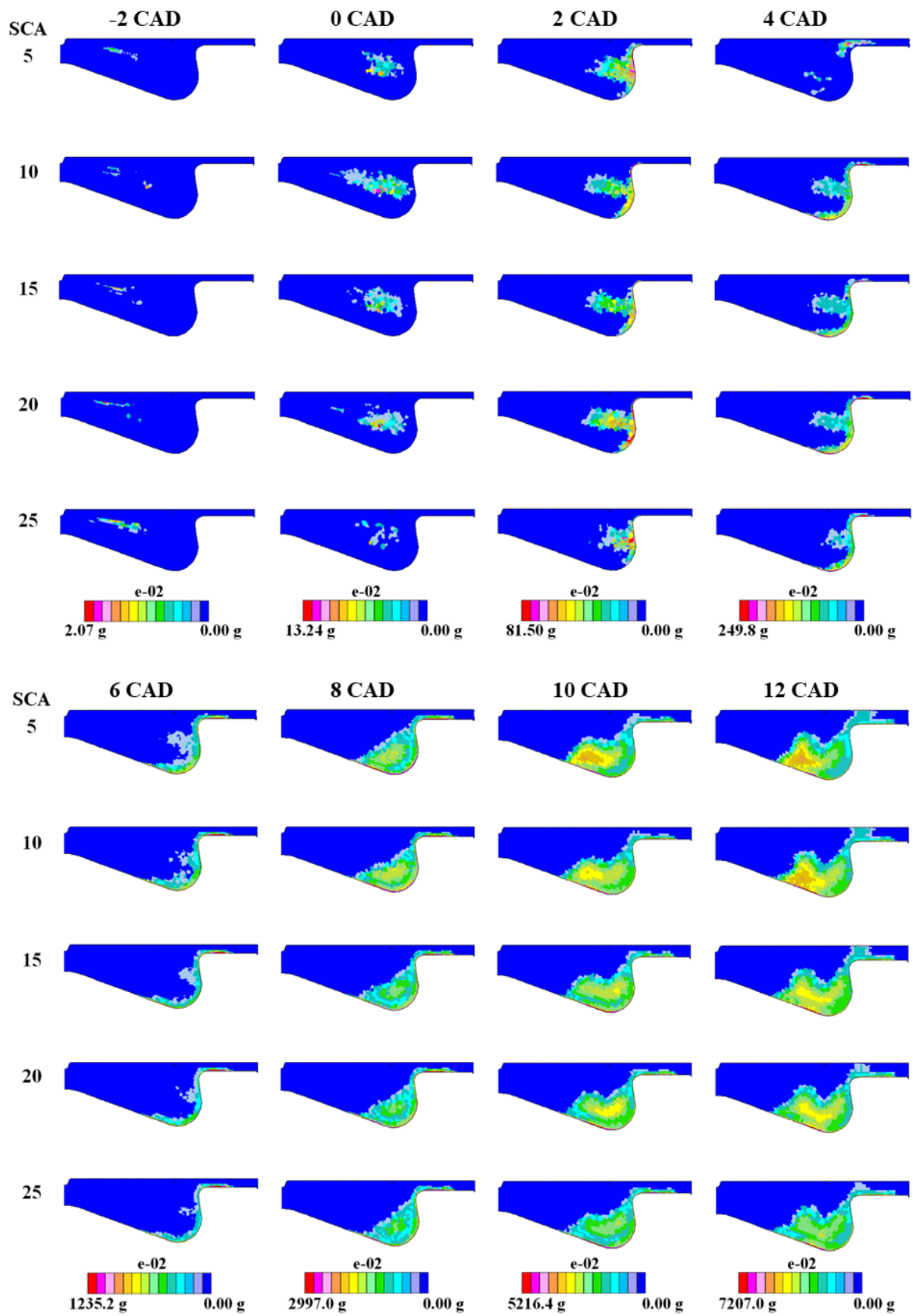


Figure 22. Soot contours.

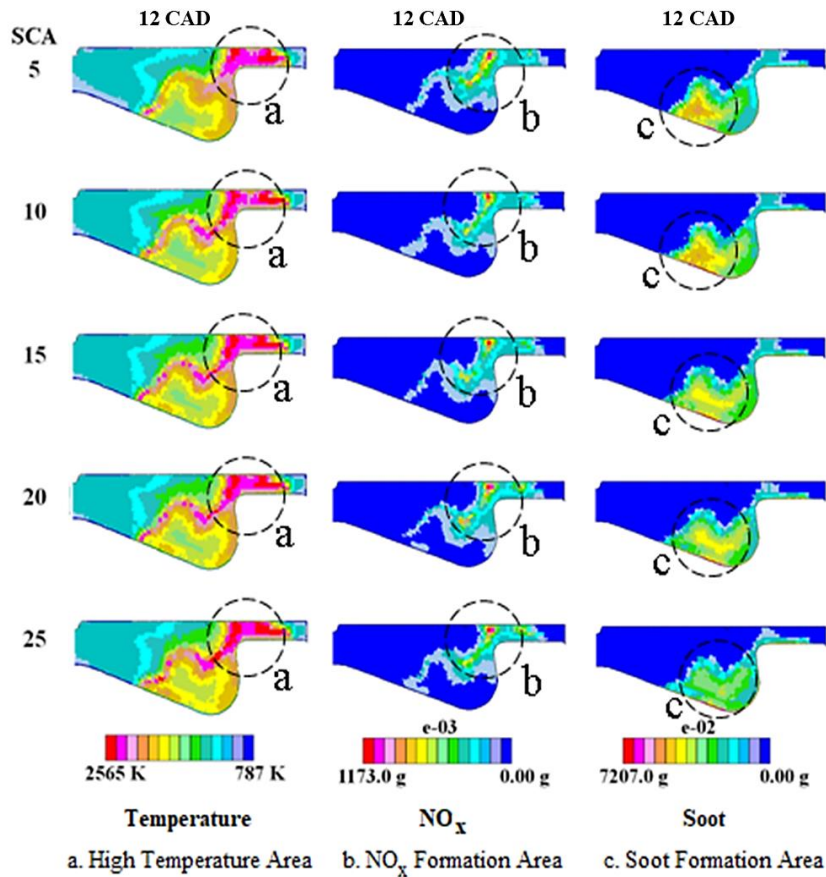


Figure 23. Comparison contour chart.

In the last part of the study, engine tests were performed using injectors with different spray cone angles. Measured performance parameters and numerical results were compared with the bar graphs for the brake mean effective pressure (BMEP), the brake specific fuel consumption (BSFC) and the brake thermal efficiency (BTE). The BMEP, the BSFC and the BTE were calculated for all spray cone angles via Star-CD. The bar graphs are given in Fig. 24, Fig. 25 and Fig. 26, respectively.

The experimental results are overall 2.32% lower than numerical results for the BMEP (Fig. 24). This is an expected situation since it is difficult to include all the test conditions in the test unit into the 3-D combustion model. Several unmeasured physical losses effect this situation such as heat loss, frictional loss at manifolds, heat loss from engine, etc. Therefore, all real losses are not exactly included into the 3-D in-cylinder combustion model.

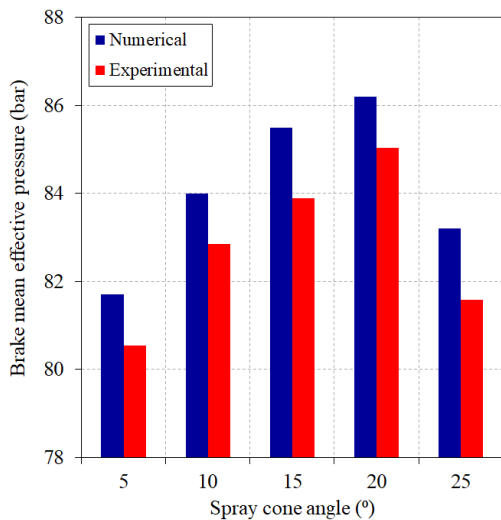


Figure 24. BMEP-SCA.

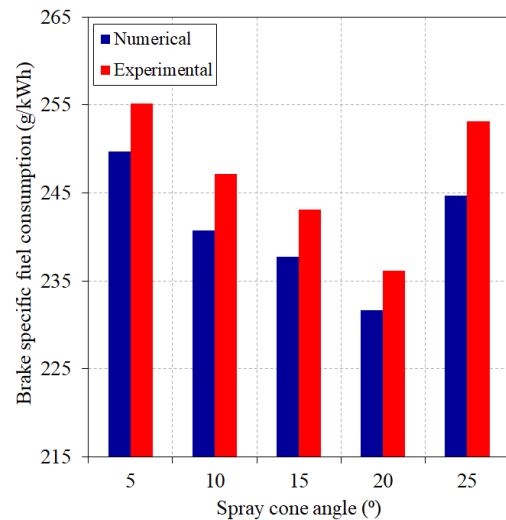
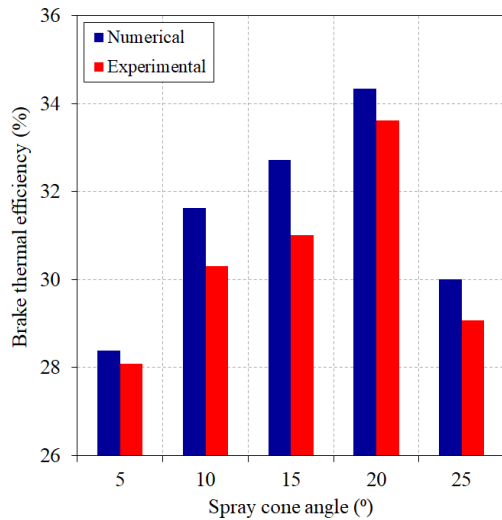


Figure 25. BSFC - SCA.

The optimum value in terms of BSFC is 20° SCA for the conditions defined when all spray cone angles are compared (Fig. 25). The BSFC numerical results are overall 2.13% lower than the experimental results. The spray cone angles compared with each other, the BSFC at tests for 20° SCA is 8.51% and 7.23% lower than 5° SCA and 25° SCA, respectively.



**Figure 26.** BTE-SCA.

The brake thermal efficiency (BTE) results are given in Fig. 26. The experimental BTE values for kerosene are overall 4.17% lower than kerosene numerical results. As can be seen from the graph for BTE at numerically, 20° SCA is 21.3% higher than 5° SCA and 14.7% higher than 25° SCA, too.

## CONCLUSIONS

In this numerical study, combustion and performance characteristics of a direct injection commercial engine were determined with respect to spray cone angles for kerosene usage. The study revealed how important the spray cone angle is for direct ignition engine combustion and performance characteristics. The 3-D in-cylinder combustion CFD model was built in Star-CD/es-ice software and temperature, OH, NO<sub>x</sub> and soot formation were examined with respect to closed cycle crank angle range for five different spray cone angle. The experimental tests were also performed using injectors with different spray cone angles. The BMEP, BSFC and BTE measurements were performed at the tests. In addition, the numerical and experimental results were compared. The optimum spray cone angle for the operating conditions specified in the kerosene usage was determined to be 20° SCA.

Findings for kerosene at different spray cone angles are summarized below.

- The in-cylinder pressure at 20° SCA is 15.8% higher than 5° SCA.
- The temperature in-cylinder increases to 5°-20° SCA while the highest temperature in-cylinder rises up from 1620 to 1720 K.
- The dissipation for 20° SCA is 43.5% lower than 5° SCA.
- The heating transfer coefficient on wall values climb from 2688 W/m<sup>2</sup>K to 3037 W/m<sup>2</sup>K when the spray cone angle increases.
- The indicated mean effective pressure at 20° SCA was calculated as 4.06% and 3.41% higher than 5° SCA and 25° SCA, respectively.
- The indicated power at 20° SCA was calculated as 7.98% and 6.72% higher than 5° SCA and 25° SCA, respectively.
- The CO<sub>2</sub> formation at 20° SCA is overall 24.3% higher than 5° SCA.
- The CO formation at 20° SCA is 7.8% lower than 5° SCA and 17.2% lower than 25° SCA.
- The OH formation at 25° SCA is 42.8% higher than 5° SCA.
- The NO<sub>x</sub> formation for 25° SCA is higher 51.2% than 5° SCA and 19.2% lower than 25° SCA.
- The soot formation at 20° SCA is overall 24.8% lower than 5° SCA.
- The experimental results are overall 2.32% lower than numerical results for the BMEP.
- The BSFC at tests for 20° SCA is 8.51% and 7.23% lower than 5° SCA and 25° SCA, respectively.
- The experimental BTE values for kerosene are overall 4.17% lower than kerosene numerical results.
- As the spray cone angle increased, the indicated power and the indicated mean effective pressure parabolic behavior.
- The temperature, thermal dissociation and NO<sub>x</sub> raised up with increasing spray cone angle.

## ACKNOWLEDGEMENTS

Author thanks to Delphi Technologies, Luxembourg.

## REFERENCES

- Agarwal A. K. and Chaudhury V. H., 2012, Spray Characteristics of Biodiesel/Blends in a High Pressure Constant Volume Spray Chamber, *Exp. Therm. Fluid Sci.*, 42, 212-218.
- Aleiferis P.G., Serras-Pereira J., Van Romunde Z., Caine J. and Wirth M., 2010, Mechanisms of Spray Formation and Combustion from a Multi-Hole Injector with E85 and Gasoline, *Combustion and Flame*, 157, 735-756.

- Arrègle J., Pastor J. V. and Ruiz S., 1999, The Influence of Injection Parameters on Diesel Spray Characteristics, *SAE Tech. Paper*, No. 1999-01-0200.
- Bai C. and Gosman A. D., 1995, Development of Methodology for Spray Impingement Simulation, *SAE Tech. Paper*, No. 950283.
- Battistoni M. and Grimaldi C. N., 2012, Numerical Analysis of Injector Flow and Spray Characteristics from Diesel Injectors using Fossil and Biodiesel Fuels, *Applied Energy*, 97, 656-666.
- CD-Adapco CD-Meth., 2016, *Star-CD Methodology*, Version 4.26.
- CD-Adapco Star-CD, 2016, *Star-CD/es-ice User Guide*, Version 4.26.
- CD-Adapco, 2016, *Star Methodology for Internal Combustion Engine Applications*, Version 4.26.
- Chen P. C., Wang W. C., Roberts W. L. and Fang T., 2013, Spray and Atomization of Diesel Fuel and Its Alternatives from a Single-Hole Injector Using a Common Rail Fuel Injection System, *Fuel*, 103, 850-861.
- Chen S. K. and Lefebvre A. H., 1994, Spray Cone Angles of Effervescent Atomizers, *Atomization and Sprays*, 4.
- Dec J. E., 1997, A Conceptual Model of D.I. Diesel Combustion Based on Laser-Sheet Imaging, *SAE Paper*, No. 970873.
- Delacourt E., Desmet B. and Besson B., 2005, Characterisation of Very High Pressure Diesel Sprays Using Digital Imaging Techniques, *Fuel*, 84, 859-867.
- Dent J. C., 1971, A Basis for the Comparison of Various Experimental Methods for Studying Spray Penetration, *SAE Trans.*, 80, 1881-1884.
- Desantes J. M., Payri R., Garcia J. M. and Salvador F. J., 2007, A Contribution to the Understanding of Isothermal Diesel Spray Dynamics, *Fuel*, 86, 1093-1101.
- Doudou A., 2005, Turbulent Flow Study of an Isothermal Diesel Spray Injected by a Common Rail System, *Fuel*, 84, 287-298.
- Heywood J. B., 1988, *Internal Combustion Engine Fundamentals*, McGraw-Hill College.
- Hiroyasu H. and Arai M., 1990, Structure of Fuel Sprays in Diesel Engines, *SAE Paper*, No. 900475.
- Hossainpour S. and Binesh A.R., 2009, Investigation of Fuel Spray Atomization in a DI Heavy-Duty Diesel Engine and Comparison of Various Spray Breakup Models, *Fuel*, 88, 799-805.
- Huh, K. Y., 1991, A Phenomenological Model of Diesel Spray Atomization, *In Proc. of The International Conf. on Multiphase Flows' 91-Tsukuba*, Tsukuba.
- Hwang J. S., Ha J. S. and Na S. Y., 2003, Spray Characteristics of DME in Conditions of Common Rail Injection System (II), *Int. J. Autom. Tech.*, 4, 119-124.
- Juslin L., Antikainen O., Merkkü P. and Yliruusi J., 1995, Droplet size measurement: I. Effect of Three Independent Variables on Droplet Size Distribution and Spray Angle from a Pneumatic Nozzle, *Int. J. Pharm.*, 123, 247-256.
- Kannaiyan K. and Sadr R., 2014, Experimental Investigation of Spray Characteristics of Alternative Aviation Fuels, *Energy Conv. Management*, 88, 1060-1069.
- Kim K., Kim D., Jung Y. and Bae C., 2013, Spray and combustion characteristics of gasoline and diesel in a direct injection compression ignition engine, *Fuel*, 109, 616-626.
- Kim M. Y. and Lee C. S., 2007, Effect of a Narrow Fuel Spray Angle and a Dual Injection Configuration on the Improvement of Exhaust Emissions in a HCCI Diesel Engine, *Fuel*, 86, 2871-2880.
- Kostas J., Honnery D. and Soria J., 2009, Time Resolved Measurements of the Initial Stages of Fuel Spray Penetration, *Fuel*, 88, 2225-2237.
- Langrish T. A. and Zbicinski I., 1994, The Effects of Air Inlet Geometry and Spray Cone Angle on The Wall Deposition Rate in Spray Dryers, *Chemical Eng. Res. Des.*, 72, 420-430.
- Liu J., Zhang X. Q., Li Q. L. and Wang Z. G., 2013, Effect of Geometric Parameters on the Spray Cone Angle In the Pressure Swirl Injector, *Proc. Inst. Mech. Eng. Part G: J. Aerospace Eng.*, 227, 342-353.
- Mahle GmbH, 2012, *Pistons and Engine Testing*, ATZ/MTZ-Fachbuch.
- Mang T., Dresel W. and Wiley, J., 2007, *Lubricants and Lubrication*, Wiley-Vch., Weinheim, Germany.
- Miller R., Davis G., Lavoie G., Newman C. and Gardner T., 1998, A Super-Extended Zel'dovich Mechanism for NO<sub>x</sub> Modeling and Engine Calibration, *SAE Tech. Paper*, No. 980781.
- Mitroglou N., Nouri J.M., Gavaises M. and Arcoumanis C., 2006, Spray Characteristics of a Multi-Hole Injector

- for Direct-Injection Gasoline Engines, *Int. J. Engine Research*, 7, 255-270.
- Naber J. and Siebers D. L., 1996, Effects of Gas Density and Vaporisation on Penetration and Dispersion of Diesel Sprays, *SAE Paper*, No. 960034.
- Nakamura M., Nishioka D., Hayashi J. and Akamatsu F., 2011, Soot Formation, Spray Characteristics, and Structure of Jet Spray Flames Under High Pressure, *Combustion and Flame*, 158, 1615-1623.
- Ohrn T. R., Senser D. W. and Lefebvre A. H., 1991, Geometric Effects on Spray Cone Angle for Plain-Orifice Atomizers, *Atomization and Sprays*, 1.
- Park S. H., Kim H. J., Suh H. K. and Lee C. S., 2009, Atomization and Spray Characteristics of Bioethanol and Bioethanol Blended Gasoline Fuel Injected Through a Direct Injection Gasoline Injector, *Int. J. Heat Fluid Flow*, 30, 1183-1192.
- Park S. H., Yoon S. H. and Lee C. S., 2011, Effects of Multiple-Injection Strategies on Overall Spray Behavior, Combustion, and Emissions Reduction Characteristics of Biodiesel Fuel, *Applied Energy*, 88, 88-98.
- Patterson M. A. and Reitz R. D., 1998, Modeling the Effects of Fuel Spray Characteristics on Diesel Engine Combustion and Emission, *SAE Trans.*, 27-43.
- Payri R., Garcia J. M., Salvador F. J. and Gimeno J., 2005, Using Spray Momentum Flux Measurements to Understand the Influence of Diesel Nozzle Geometry on Spray Characteristics, *Fuel*, 84, 551-561.
- Raju V. R. K. and Rao S. S., 2015, Effect of Fuel Injection Pressure and Spray Cone Angle in DI Diesel Engine Using CONVERGENT CFD Code, *Proc. Eng.*, 127, 295-300.
- Rashad M., Yong H. and Zekun Z., 2016, Effect of Geometric Parameters on Spray Characteristics of Pressure Swirl Atomizers, *Int. J. Hyd. Energy*, 41, 15790-15799.
- Reitz R. D. and Diwakar R., 1986, Effect of Drop Breakup on Fuel Sprays, *SAE Tech. Paper*, No. 860469.
- Roisman I. V., Araneo L. and Tropea C., 2007, Effect of Ambient Pressure on Penetration of a Diesel Spray, *Int. J. Multiphase Flow*, 33, 904-920.
- Skogsberg M., Dahlander P., Lindgren R. and Denbratt I., 2005, Effects of Injector Parameters on Mixture Formation for Multi-Hole Nozzles in a Spray-Guided Gasoline DI Engine, *SAE Tech. Paper*, No. 2005-01-0097.
- Sovani S. D., Chou E., Sojka P. E., Gore J. P., Eckerle W. A. and Crofts J. D., 2001, High Pressure Effervescent Atomization: Effect of Ambient Pressure on Spray Cone Angle, *Fuel*, 80, 427-435.
- Suh H. K., Park S. W. and Lee C.S., 2007, Effect of Piezodriven Injection System on the Macroscopic and Microscopic Atomization Characteristics of Diesel Fuel Spray, *Fuel*, 86, 2833-2845.
- Varde K. S., Popa D. M. and Varde L. K., 1984, Spray Angle and Atomization in Diesel Sprays, *SAE Trans.*, 779-787.
- Verhoeven D., Vanhemelryck J. L. and Baritaud T., 1998, Macroscopic and Ignition Characteristics of High Pressure Sprays of Single-Component Fuels, *SAE Paper*, No. 981069.
- Von Berg E., Edelbauer W., Alajbegovic A., Tatschl R., Volmajer M., Kegl B. and Ganippa L.C., 2005, Coupled Simulations of Nozzle Flow, Primary Fuel Jet Breakup, and Spray Formation, *J. Eng. Gas Turbine and Power*, 127, 897-908.
- Wakuri Y., Fujii M., Amitani T. and Tsuneya R., 1960, Studies of the Penetration of Fuel Spray in a Diesel Engine, *Bull. Japan Soc. Mech. Eng.*, 3, 9.
- Wang X., Huang Z., Kuti O. A., Zhang W. and Nishida K., 2010, Experimental and Analytical Study on Biodiesel and Diesel Spray Characteristics Under Ultra-High Injection Pressure, *Int. J. Heat Fluid Flow*, 31, 659-666.
- Watanabe H., Suwa Y., Matsushita Y., Morozumi Y., Aoki H., Tanno S. and Miura T., 2007, Spray Combustion Simulation Including Soot and NO Formation, *Energy Conv. Management*, 48, 2077-2089.